International Journal of Plasticity 49 (2013) 1–15

Contents lists available at SciVerse ScienceDirect

International Journal of Plasticity

journal homepage: www.elsevier.com/locate/ijplas

Extended expanding cavity model for measurement of flow properties using instrumented spherical indentation

Seung-Kyun Kang [a], Young-Cheon Kim [a], Kug-Hwan Kim [a], Ju-Young Kim [b,*], Dongil Kwon [a]

[a] Department of Materials Science and Engineering, Seoul National University, Seoul 151-744, Republic of Korea
[b] School of Mechanical & Advanced Materials Engineering, UNIST, Ulsan 689-798, Republic of Korea

ARTICLE INFO

Article history:
Received 26 June 2012
Received in final revised form 20 December 2012
Available online 15 March 2013

Keywords:
Instrumented indentation
B. Elastic-plastic material
B. Metallic material
C. Mechanical testing

ABSTRACT

We propose an extended expanding cavity model (ECM) in instrumented spherical indentation to evaluate flow properties measured in uniaxial mechanical testing. We describe the mean pressure of the projected surface from radial stress at the hemispherical core boundary with a scaling factor for strain-hardening metals. Plastic constraint factors determined by the strain-hardening exponent, yield strain and scaling factor successfully illustrate flow stress–strain points in uniaxial tension tests. We suggest a novel way to determine the strain-hardening exponent from the ratio of indentation loading slope, and a modified Meyer relation to measure yield strengths.

1. Introduction

Flow properties describing plasticity in uniaxial mechanical testing are indispensable in characterizing and predicting deformation and fracture. In conventional uniaxial tensile testing, standards or precise procedures for sample preparation and testing are required. However, tensile testing can be difficult or challenging when (1) destructive preparation of sample is infeasible and (2) testing is limited to local volumes such as a single grain in polycrystalline materials or weld regions with sharp mechanical-property gradients (Kim et al., 2006a; Shi et al., 2008; Yang et al., 2011). With these limitations on tensile testing, instrumented indentation testing (IIT) has been investigated as a tool to evaluate flow properties in tensile testing because of its simple and nondestructive sample preparation and testing (Dao et al., 2001; Herbert et al., 2001; Buclille et al., 2003; Anand and Ames, 2006; Kim et al., 2006a; Lee et al., 2005; Antunes et al., 2007; Gouldstone et al., 2007; Haj-Ali et al., 2008).

In the 1950s, Tabor (1951), on the basis of experiments on metals, suggested the following relations between flow stress and strain in uniaxial tension and parameters in spherical indentation:

$$\sigma_t = \frac{p_m}{\psi} = \frac{1}{\psi} \cdot \frac{L}{A}, \tag{1}$$

$$\varepsilon_t = 0.2\frac{a}{R}, \tag{2}$$

where σ_t and ε_t are flow stress and strain in uniaxial tension, p_m is mean indentation pressure, ψ is the plastic constraint factor (taken as 3 in Tabor's work), L is the indentation load, a and A are the contact radius and cross-sectional contact area

* Corresponding author. Tel.: +82 52 217 2334; fax: +82 52 217 2309.
E-mail address: juyoung@unist.ac.kr (J.-Y. Kim).

0749-6419/$ - see front matter
http://dx.doi.org/10.1016/j.ijplas.2013.02.014

of the indent and R is the radius of the spherical indenter. Since Tabor's work, extensive research has been carried out to investigate these relations. Ahn and Kwon (2001) modified the definition of flow strain to be average loading-directional shear strain beneath the indenter, and evaluated the plastic flow properties for power-law-hardening metals. Matthews (1980), Taljat et al. (1998), and Sundararajan and Tirupataiah (2006) have suggested that the plastic constraint factor in Eq. (1) is a function of the strain-hardening exponent in uniaxial tensile testing. Recently the investigation of flow stress and indentation mean pressure is extended to plastically strain graded materials (Gao, 2006; Gao et al., 2006; Shi et al., 2008; Branch et al., 2011a,b), metallic glasses (Fornell et al., 2009), and composite materials (Veprek-Heijman et al., 2009; Ma et al., 2012) and the indentation tests with wedge indenter (Kysar and Saito, 2011). These approaches are generally called representative stress–strain methods using instrumented indentations.

The representative stress–strain method is based on correlating mechanical responses in uniaxial tension and spherical indentation, and thus, understanding the stress field in spherical indentation is essential. To explain the stress field beneath spherical indenter, Johnson (1985) suggested the expanding cavity model (ECM), which applies Hill's spherical cavity model in contact mechanics to spherical indentation. Fig. 1 is a schematic diagram of the stress field in the ECM. Hydrostatic pressure is assumed to be applied to a hemispherical core corresponding to contact radius a, and the stress field in plastic region ranging from the contact radius a to plastic zone size c is explored. In the plastic zone, the ECM assumes perfect plasticity with no strain-hardening.

Although the ECM has been widely used to explain the stress field in spherical indentation, such simple assumptions as hydrostatic pressure in the hemispherical core and perfect plasticity in the plastic deformation region are likely to be unrealistic. Here we suggest an expanded ECM for describing the stress fields in spherical indentation, so that flow properties such as yield strength and strain-hardening exponent can be evaluated only by spherical IIT. In the expanded ECM, we take into account extra hardening at the core in Fig. 1, which yields good agreement between the flow stress in tension tests and representative stress–strain points in spherical IIT. We propose unique analytic models to measure flow properties, strain-hardening exponent and yield strength from the representative stress–strain points.

2. Experiments

We prepared 13 metallic alloys: aluminum alloys Al6061 and Al7075, carbon steels S45C, SK4, SKS3, SUJ2, API X100, stainless steels STS303F, STS316L, STS403, STS420J2, and titanium alloys Ti–6Al–4 V, and Ti–7Al–4Mo. Cylindrical tensile samples with gauge length 25 mm and diameter 6 mm were prepared according to ASTM E8-04 (2002). Uniaxial tensile tests were performed at crosshead speed 0.5 mm/min by Instron 5582 (Instron Inc., Grove City, PA, USA). For instrumented spherical indentation tests, cubic samples of side 5 mm were prepared and one side of the sample was polished with 1 μm alumina powder. IITs were carried out using AIS 3000 (Frontics Inc., Seoul, Korea) with a spherical indenter of radius 250 μm. Indentation depths were every 10 μm from 10 μm to 100 μm, loading and unloading rates were 1 mm/min, and we performed five repeatable tests for each point. To evaluate the mean pressure accurately, the cross-sectional contact area was measured from the residual impression. After each indentation test, the projected area as a cross-sectional contact area was measured by optical microscope (Kim et al., 2006b; Liu et al., 2008; Kang et al., 2012). An ultrasonic pulse–echo method was used to measure sample elastic moduli.

3. Theoretical models

Expanding cavity models (ECMs) have been developed to explain indentation responses of various materials (Marsh, 1964; Samuels, 1957; Mulhearn, 1959; Johnson, 1985; Shaw and DeSalvo, 1970; Yoffe, 1982) on the basis of Hill's solution

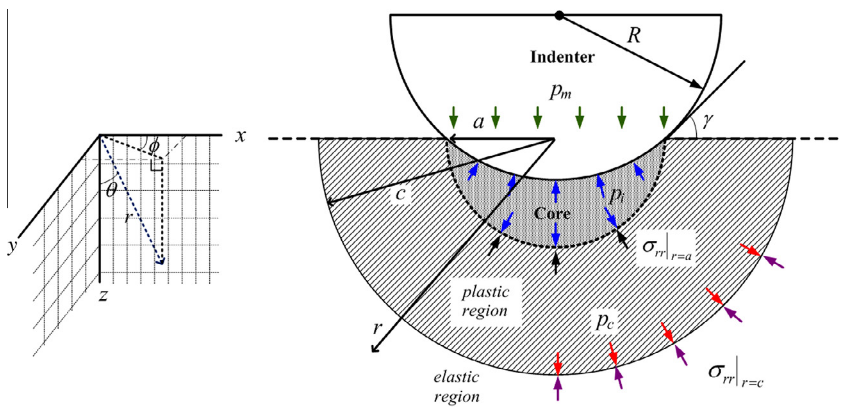

Fig. 1. Stress field in spherical indentation with the expanding cavity model (ECM) where x and y are surface plane directions and z is loading direction.

for the quasi-static expansion of an internally pressurized spherical shell of an elastic-perfectly plastic material (Hill, 1950). Early report of Samuels & Mulhearn (1957) and Mulhearn (1959) showed that displacements under surface are approximately radial from the first contact point when any blunt indenter contact, so there is hemi-spherical contours of equal strain. Johnson (1970) extended this simple model to indentation by considering a hemi-spherical core of radius a. It is assumed that the inner region of core has hydrostatic stress state and outer region of core has radial symmetrical stress state. The expanding cavity models have widely been used to describe indentation deformation for its simplicity and good predictability. However conventional models are on the basis of elastic-perfectly plastic materials, so there are reports of large violation in strain hardening materials (Tabor, 1986; Lawn, 1998). To evaluate indentation deformation of strain hardening materials finite element analysis have been used.

Akyuz and Merwin (1968) used two-dimensional stress for a cylindrical indentation, and Hardy et al. (1971), Dumas and Baronet (1971), Lee et al. (1972) and Skalski (1979) considered the development of the plastic zone as the load is increased. Analytical solutions were also suggested by Chadwick (1959), Durban and Baruch (1976), Chiang et al. (1982), Bigoni and Laudiero (1989) and Lubliner (1990). These researches mainly concerned internal pressure of cavity which is suggested in Johnson's model. They gave good analytical formulation between internal pressure and plastic zone size. However, the relation between the plastic zone and the mechanical properties was not carefully considered.

One recent analysis was performed by Gao et al. (2006). Gao et al.'s studies give solutions for an internally pressurized spherical shell of the plastic power-law hardening material under the assumptions of infinitesimal deformations, isotropic hardening, and incompressibility. The von Mises yield criterion and Hencky's deformation theory (1924) which is valid for an isotropic materials under radial loading were used for following derivations.

In elastic region, according to Lame solution, the radial stress (σ_{rr}), the angular and axial stresses ($\sigma_{\theta\theta}, \sigma_{\varphi\varphi}$) in spherical polar coordinates are,

$$\sigma_{rr} = -p_i\left(\frac{a}{r}\right)^3, \quad \sigma_{\theta\theta} = \sigma_{\varphi\varphi} = -\frac{p_i}{2}\left(\frac{a}{r}\right)^3, \tag{3}$$

where p_i is the pressure at the core, a is contact radius, r is the radial distance from the center of the hemisphere.

On the elastic–plastic boundary ($r = c$), we can get Eq. (3) as follows:

$$\sigma_{rr} = -p_c\left(\frac{c}{r}\right)^3, \quad \sigma_{\theta\theta} = \sigma_{\varphi\varphi} = -\frac{p_c}{2}\left(\frac{c}{r}\right)^3, \tag{4}$$

where p_c and c are the pressure at the boundary and the size of the plastic zone in Fig. 1. And the stress components in Eq. (4) should satisfy the yield condition. The stress state can be separated as fully hydrostatic tension state and deviatoric compression state

$$\begin{pmatrix} \sigma_{rr} & 0 & 0 \\ 0 & \sigma_{\theta\theta} & 0 \\ 0 & 0 & \sigma_{\varphi\varphi} \end{pmatrix} = \begin{pmatrix} \sigma_{\theta\theta} & 0 & 0 \\ 0 & \sigma_{\theta\theta} & 0 \\ 0 & 0 & \sigma_{\theta\theta} \end{pmatrix} + \begin{pmatrix} \sigma_{rr} - \sigma_{\theta\theta} & 0 & 0 \\ 0 & 0 & 0 \\ 0 & 0 & 0 \end{pmatrix}. \tag{5}$$

Inserting Eq. (4) into the yield condition ($\sigma_{\theta\theta} - \sigma_{rr} = \sigma_y$, where σ_y is yield strength) gives p_c as 2/3 σ_y. We can rewrite Eq. (4) as:

$$\sigma_{rr} = -\frac{2\sigma_y}{3}\left(\frac{c}{r}\right)^3, \quad \sigma_{\theta\theta} = \sigma_{\varphi\varphi} = -\frac{\sigma_y}{3}\left(\frac{c}{r}\right)^3 \quad (c < r). \tag{6}$$

For Holloman hardening materials, we can describe the true stress–strain relation by

$$\sigma_t = E\varepsilon_t \quad (\varepsilon \le \varepsilon_y), \tag{7a}$$

$$\sigma_t = K\varepsilon_t^n \quad (\varepsilon \ge \varepsilon_y), \tag{7b}$$

where E, K, and n are elastic modulus, strength coefficient, and strain-hardening exponent in uniaxial tension, respectively.

The governing equations in a stress formulation of Hencky's deformation theory include the equilibrium equation

$$\frac{\partial\sigma_{rr}}{\partial r} + \frac{1}{r}(2\sigma_{rr} - \sigma_{\theta\theta} - \sigma_{\varphi\varphi}) = \frac{\partial\sigma_{rr}}{\partial r} + \frac{2}{r}(\sigma_{rr} - \sigma_{\theta\theta}) = 0, \tag{8}$$

the compatibility equation

$$\frac{\partial\varepsilon_{\theta\theta}}{\partial r} = \frac{\varepsilon_{rr} - \varepsilon_{\theta\theta}}{r}, \tag{9}$$

where ε_{rr}, $\varepsilon_{\theta\theta}$, and $\varepsilon_{\varphi\varphi}$ are the radial, angular, and axial directional strains in spherical coordinate, and the constitutive equation (Gao, 2006; Gao et al., 2006)

$$\varepsilon_{rr} = -\frac{\varepsilon_t}{\sigma_t}(\sigma_{\theta\theta} - \sigma_{rr}), \tag{10a}$$

$$\varepsilon_{\theta\theta} = \varepsilon_{\varphi\varphi} = \frac{1}{2}\frac{\varepsilon_t}{\sigma_t}(\sigma_{\theta\theta} - \sigma_{rr}). \tag{10b}$$

The boundary conditions are

$$\sigma_{rr}|_{r=a} = -p_i, \tag{11a}$$

$$\sigma_{rr}|_{r=c} = -p_c, \tag{11b}$$

$$\varepsilon_{rr}|_{r=c} = \varepsilon_y = \sigma_y/E. \tag{11c}$$

The von Mises yield criterion (Tresca yield criterion leads the same result) will be expressed by

$$\sigma_{\theta\theta} - \sigma_{rr} = \sigma_t = K\varepsilon_t^n. \tag{12}$$

The strain distribution can be found as follows. Using Eq. (12) in Eq. (10) gives

$$\varepsilon_{rr} = -\varepsilon_t, \quad \varepsilon_{\theta\theta} = \frac{1}{2}\varepsilon_t. \tag{13}$$

From Eq. (9), we can get

$$\frac{\partial\varepsilon_{rr}}{\varepsilon_{rr}} = -3\frac{dr}{r}. \tag{14}$$

Integrating Eq. (14) from a to r gives

$$\varepsilon_{rr} = A\frac{a^3}{r^3}, \tag{15}$$

where A is the constant of integration, which means the true strain at $r = a$.

Inserting Eqs. (11c) and (13) into Eq. (15) gives

$$A = \frac{\sigma_y}{E}\frac{c^3}{a^3}. \tag{16}$$

Inserting Eq. (16) into Eq. (15), and using Eq. (13), we can get strain distributions as follows:

$$\varepsilon_{rr} = -\frac{\sigma_y}{E}\frac{c^3}{r^3}, \tag{17a}$$

$$\varepsilon_{\theta\theta} = \varepsilon_{\varphi\varphi} = \frac{1}{2}\frac{\sigma_y}{E}\frac{c^3}{r^3}. \tag{17b}$$

The radial displacement is

$$u_{rr} = \int \varepsilon_{rr} dr = \frac{1}{2}\frac{\sigma_y}{E}\frac{c^3}{r^2}. \tag{18}$$

The calculation of stress distribution is more complex. Inserting Eq. (12) into Eq. (8) gives

$$\frac{d\sigma_{rr}}{dr} = \frac{2\sigma_t}{r}. \tag{19}$$

Using Eqs. (7) and (17), Eq. (19) can be changed to

$$\frac{d\sigma_{rr}}{dr} = \frac{2K}{r}\left(\frac{\sigma_y}{E}\frac{c^3}{r^3}\right)^n = 2K\left(\frac{\sigma_y}{E}c^3\right)^n \cdot \frac{1}{r^{3n+1}}. \tag{20}$$

Integrating from a to r gives

$$\sigma_{rr} = 2K\left(\frac{\sigma_y}{E}c^3\right)^n \cdot \left(\frac{1}{-3n}\right)\frac{1}{r^{3n}} + B, \tag{21}$$

where B is the constant of integration.

Inserting the boundary condition (Eq. (11b)) into Eq. (21) gives

$$B = -p_c + \frac{2K}{3n}\left(\frac{\sigma_y}{E}\right)^n. \tag{22}$$

From the solution in the elastic region (Eq. (6)), the pressure at the elastic–plastic boundary (p_c) is $2/3\sigma_y$. Thus, Eq. (21) yields

$$\sigma_{rr} = -\frac{2}{3}\sigma_y + \frac{2K}{3n}\left(\frac{\sigma_y}{E}\right)^n\left(1 - \frac{c^{3n}}{r^{3n}}\right). \tag{23}$$

As mentioned above, for continuity of hardening behavior at $\varepsilon = \varepsilon_y$, the strength coefficient K will be

$$K = \left(\frac{E}{\sigma_y}\right)^n \cdot \sigma_y. \tag{24}$$

Substituting Eq. (24) into Eq. (23) gives

$$\sigma_{rr} = -\frac{2}{3}\sigma_y + \frac{2\sigma_y}{3n}\left(1 - \frac{c^{3n}}{r^{3n}}\right) = -\frac{2\sigma_y}{3}\left(1 + \frac{1}{n}\left(\frac{c^{3n}}{r^{3n}} - 1\right)\right). \tag{25}$$

Also, from Eqs. (8) and (25), the circumferential stress can be obtained as

$$\sigma_{\theta\theta} = \sigma_{\varphi\varphi} = \frac{r}{2}\frac{d\sigma_{rr}}{dr} + \sigma_{rr} = -\frac{2\sigma_y}{3}\left[1 - \frac{1}{n} + \frac{1}{n}\left(1 - \frac{3n}{2}\right)\frac{c^{3n}}{r^{3n}}\right]. \tag{26}$$

The volume of material displaced by the indenter is assumed to be accommodated by the radial expansion of the hemispherical core. For the spherical indenter, the assumed conservation of volume of the core yields

$$\pi a^2 dh = 2\pi a^2 du_r|_{r=a}. \tag{27}$$

From the relation between contact depth h and contact radius ($h = R - \sqrt{R^2 - a^2}$), we have

$$dh = \frac{ada}{\sqrt{R^2 - a^2}} = \frac{a}{R}da\left(1 + \frac{1}{2}\frac{a^2}{R^2} + \cdots\right), \tag{28}$$

with all nonlinear terms truncated. This approximation works well for spherical indentations with small a/R.

From Eq. (18), it follows that the rate of change of the radial expansion at any r in the plastic zone with respect to c is

$$\frac{du_r|_{r=a}}{dc} = \frac{3}{2}\frac{\sigma_y}{E}\frac{c^2}{r^2}, \tag{29}$$

which gives

$$du_r|_{r=a} = \frac{3}{2}\frac{\sigma_y}{E}\frac{c^2}{a^2}dc. \tag{30}$$

Inserting Eqs. (28) and (30) into Eq. (27) and direct integration yield

$$c = \sqrt[3]{\frac{1}{4}\frac{E}{\sigma_y}\frac{a}{R}}a \tag{31}$$

Thus, the radial strain and stress (Eqs. (17) and (25)) can be rewritten as follows:

$$\varepsilon_{rr} = -\frac{1}{4}\frac{a}{R}\frac{a^3}{r^3}, \tag{32}$$

$$\sigma_{rr} = -\frac{2\sigma_y}{3}\left(1 + \frac{1}{n}\left(\frac{1}{4}\frac{E}{\sigma_y}\frac{a}{R}\frac{a^{3n}}{r^{3n}} - 1\right)\right), \tag{33}$$

and the pressure of core p_i and its strain ($\varepsilon_{rr}|_{r=a}$) can be obtained as

$$p_i = -\sigma_{rr}|_{r=a} = \frac{2\sigma_y}{3}\left(1 + \frac{1}{n}\left(\frac{1}{4}\frac{E}{\sigma_y}\frac{a}{R} - 1\right)\right), \tag{34}$$

$$\varepsilon_{rr}|_{r=a} = -\frac{\sigma_y}{E}\frac{c^3}{a^3} = -\frac{1}{4}\frac{a}{R} = -0.25\sin\gamma, \tag{35}$$

where γ is the contact angle between the indenter and the plane surface of the sample.

Eq. (34) implies that the mean pressure (or hardness) depends not only on the material properties such as E, σ_y, n, but also on the indentation size a and the indenter radius R.

4. Results and discussion

4.1. Expanded ECM with extra-hardened core

In the derivation of ECM, it should be noted that the actual mean pressure at the cross-sectional material surface p_m is not equal to the radial directional pressure at the core p_i. This implies two points. First, the actual cavity occupied by the indenter is not the hemispherical cavity assumed in the model. The region between the volume occupied by the indenter and the hemispherical core (dotted region in Fig. 1) experiences plastic deformation, and this may cause difference in stress distribution at the core boundary ($r = a$). Second, the mean pressure p_m is not fully converted into radial hydrostatic pressure at the hemispherical core boundary in the ECM.

Johnson (1985) suggested the following equation for perfectly plastic materials to describe the difference between the actual mean pressure at the cross-sectional material surface p_m and radial directional pressure at the core p_i:

$$p_m = p_i + \frac{2}{3}\sigma_y. \tag{36}$$

Studman et al. (1977) suggested the following relation from the Mises criterion:

$$p_m = p_i + \frac{1}{2}\sigma_y. \tag{37}$$

These equations suggest that (1) the stress in the core is higher than at the core boundary and (2) the stress difference between the core and the core boundary is proportional to the yield stress as the stress in the plastic zone is relatively proportional to yield stress. The two equations above describe perfectly plastic materials, so an extended relation for strain-hardening materials is necessary. We suggest the following relation with scaling factor k for strain-hardening materials:

$$p_m = p_i + k\sigma_t. \tag{38}$$

The flow stress σ_t is used as in the yield conditions in the Eq. (5) instead of the yield strength. We evaluated p_m from IIT with contact area corrected by optically measured residual impression, and p_i using Eq. (34) from the yield strength and strain-hardening exponent measured in uniaxial tensile tests and elastic modulus measured by the ultrasonic pulse–echo method. We measured k using p_m and p_i in Eq. (38) for 13 metallic materials where σ_t is obtained from the flow stress on the stress–strain curve measured by tensile testing at the strain of Eq. (35).

Fig. 2 shows the relation of evaluated k and the strain-hardening exponent n, and k and the yield strain σ_y/E for three indentation depths, h/R of 0.04, 0.12, and 0.20, where h is indentation depth. k is calculated from Eq. (38). In this calculation, p_m is defined to be L/A where L is measured from indentation test and A is observed by residual impression, p_i is obtained from Eq. (35) where σ_y and n are measured in tensile tests, E is measure by ultrasonic pulse-echo method, and a is observed from residual impression. σ_t is defined as the flow stress on flow curve measured in tensile tests at the corresponding representative strain by Eq. (35). Eleven materials in this study (except for the two austenitic stainless steels, STS303F and STS316L) have k values from 0.43 to 0.83 (average value 0.61 ± 0.11) independent of n and σ_y/E. The deviation of k is expected to be restricted to about 10% because p_i is generally at least twice σ_t in the fully plastic region (Johnson, 1985; Kim et al., 2011). The dependence of k on materials may be attributed to extra strain-hardening and non-uniform stress distribution in the core, which is materials-dependent, whereas ECM assumes no strain hardening and a uniform stress distribution in the core. However, Fig. 2 shows that the extra strain-hardening is not the primary factor in the difference between p_m and p_i. In Fig. 2, k has no relation to indentation depth, i.e. the deviation in k value for three different h/R values for each material is very small. This implies that the material region between the volume occupied by the indenter and the hemispherical core has little effect on the difference between p_m and p_i since th evolume occupied by spherical indenter approaches the hemispherical core in the ECM as indentation depth increases. Moreover, k shows no trend with respect to n and σ_y/E, as shown in Fig. 2.

The exceptionally high k values of the austenitic stainless steels STS303F and STS316L are examined in terms of strain-hardening behavior and pileup. While the other 11 materials shows power-law hardening behavior, the austenite-based stainless steels are reported to show almost linear plasticity with pronounced strain-hardening even at relatively high strain, which is attributed to extra dislocation hardening due to cross-slip in austenite's FCC system (Samuel and Rodriguez, 2005; Lee et al., 2008). In Eqs (17a), (25), (31), (34), (35), which were developed on the basis of the constitutive equation of power-law-hardening materials, p_i can be underestimated since the representative stress of linear-hardening materials is generally underestimated by the power-law-hardening constitutive equation, and this can yield overestimated k values.

Another feature of the austenite-based stainless steels is the rarity of pileup due to pronounced strain-hardening (Alcala et al., 2000; Kang et al., 2012). Pileup, which is not considered in ECM, enters into the determination of mean pressure by change in contact area as well as stress distribution under indenter (Jiang et al., 2009; Hernot and Bartier, 2012). When determining mean pressure in this study, pileup is taken into account by direct measurement of the residual impression. In terms of stress distribution, pileup widens the surface contact area, resulting in dispersion of stress beneath the indenter. Compared to Hill's spherical cavity model, in which a hydrostatic pressure originates from the core center, the source stress in ECM is introduced normal to the cross section at the core center. This implies that the stress concentration is dominant toward the loading direction and that the contour line of stress distribution is bell-shaped. Because pileup is generally in-

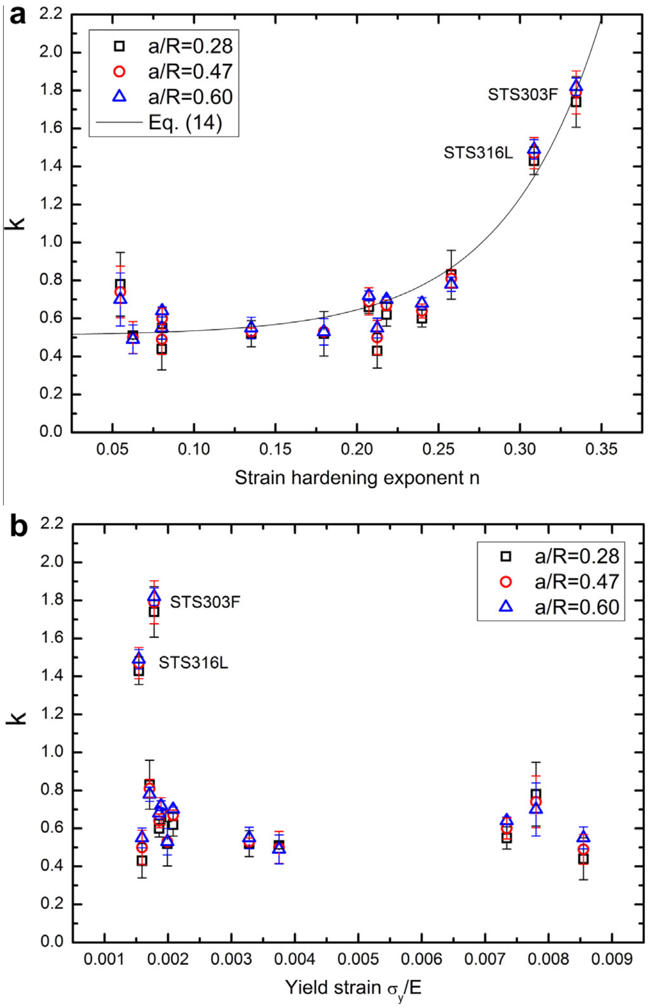

Fig. 2. Scaling factor k as a function of (a) strain-hardening exponent n and (b) yield strain σ_y/E.

versely proportional to the amount of strain-hardening, this result is in line with the finite-element analysis of Mata et al. (2006), who have shown that the shape of stress field under the indenter changes with the strain-hardening exponent, and that highly hardened materials show a bell-shaped distribution.

4.2. Plastic constraint factor

We rewrite the constraint factor by combining Eqs. (1), (7b), (34), and (38) as

$$\psi = \frac{p_m}{\sigma_t} = \frac{p_i + k\sigma_t}{K\varepsilon_t^n} = \frac{2}{3}\left(\left(1 - \frac{1}{n}\right)\left(\frac{1}{4}\frac{E}{\sigma_y}\frac{a}{R}\right)^{-n} + \left(\frac{1}{n} + \frac{3k}{2}\right)\right). \tag{39}$$

This says that the constraint factor depends on the strain-hardening exponent n, yield strain $\frac{\sigma_y}{E}$, and relative indentation depth a/R. Describing the scaling factor k by the strain-hardening exponent n eliminates one variable. For simplicity, we give the following relation between the scaling factor k and strain-hardening exponent n for 13 metals in this study by fitting an exponential curve to experimental results in Fig. 2a:

$$k = 0.5098 + 0.0048\exp\left(\frac{n}{0.0598}\right). \tag{40}$$

Using Eq. (40) yields the relation between constraint factor Ψ and relative indentation depth a/R for various values of n and $\frac{\sigma_y}{E}$ presented in Fig. 3. Fig. 3a shows the decrease in the plastic constraint factor with increasing yield strain for a fixed n of 0.20. Fig. 3b shows that the plastic constraint factor increases as strain-hardening exponent decreases for a fixed $\frac{\sigma_y}{E}$ of

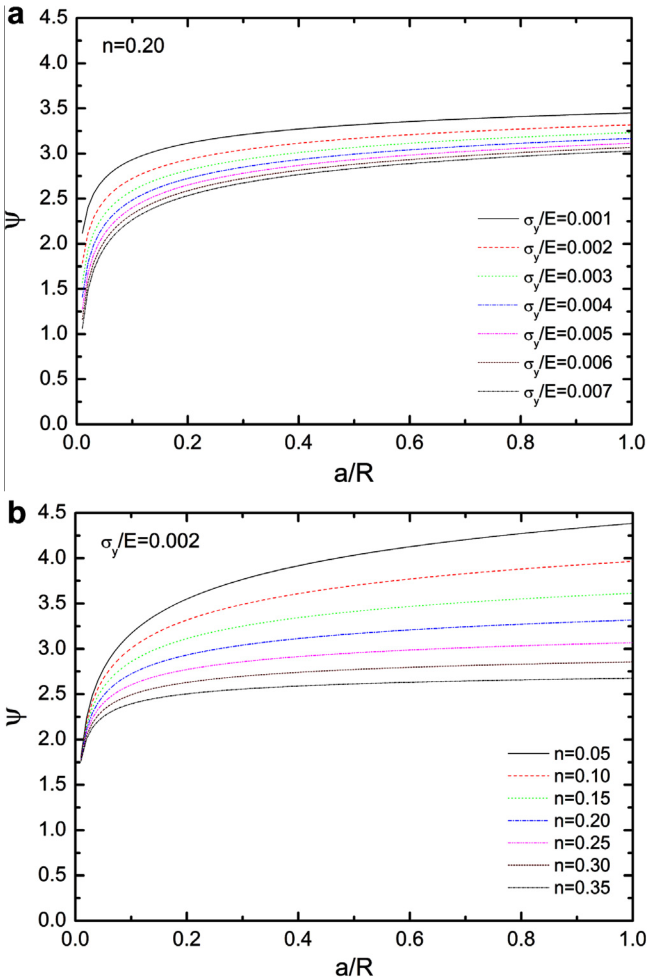

Fig. 3. Dependence of plastic constraint factor on (a) strain-hardening exponent and (b) yield strain.

0.002. The variation in the plastic constraint factor with strain-hardening exponent is found to be more pronounced than that with yield strain. The above three results can be conceptually understood by the extent of relative plastic strain at the core boundary.

Another feature shown in Fig. 3 is an increase of the plastic constraint factor as the relative indentation depth a/R increases. In general, three stages are expected in the developing stress field under the spherical indenter (Park and Pharr, 2004; Kim et al., 2011). The first stage is the elastic regime with fully elastic contact; the second is a transition regime in which plastic deformation begins and competes with elastic deformation. The third stage is the plastic regime, in which the plastic zone is fully developed and the rate of increase of the plastic zone is saturated. It is of interest that the plastic constraint factor as a function of relative indentation depth shows the saturation expected in the fully plastic regime. The criterion for relative indentation depth between elastic and transition regimes is not presented because it is relatively very shallow depth. In previous research, a saturation point is expected only in the combination of relative indentation depth and yield strain. However, Fig. 3b implies that the development of the plastic zone is affected by strain-hardening exponent as well.

Fig. 4 shows flow stresses as evaluated by Eqs. (1), (39), (40), flow strains by Eq. (35), and flow curves measured by uniaxial tensile tests. We found improved agreement between flow stress–strain points evaluated by IIT and flow curves in uniaxial tension for the newly developed model over the constant plastic constraint factor of 3. The flow stress–strain points evaluated by IIT for Al6061 and Ti–7Al–5Mo with strain-hardening exponents 0.0625 and 0.0548 respectively are remarkably improved by using the plastic constraint factor as a function of uniaxial properties in Eq. (39). As discussed above, this probably arises from the correction of the plastic constraint factor to depend on the strain-hardening exponent.

For application of Eq. (39), we need to know tensile properties such as strain-hardening exponent and yield strain. With no preliminary tensile test, i.e. only with IIT, these properties can be determined by the iteration method and representative stress–strain method (Dao et al., 2001; Herbert et al., 2001).

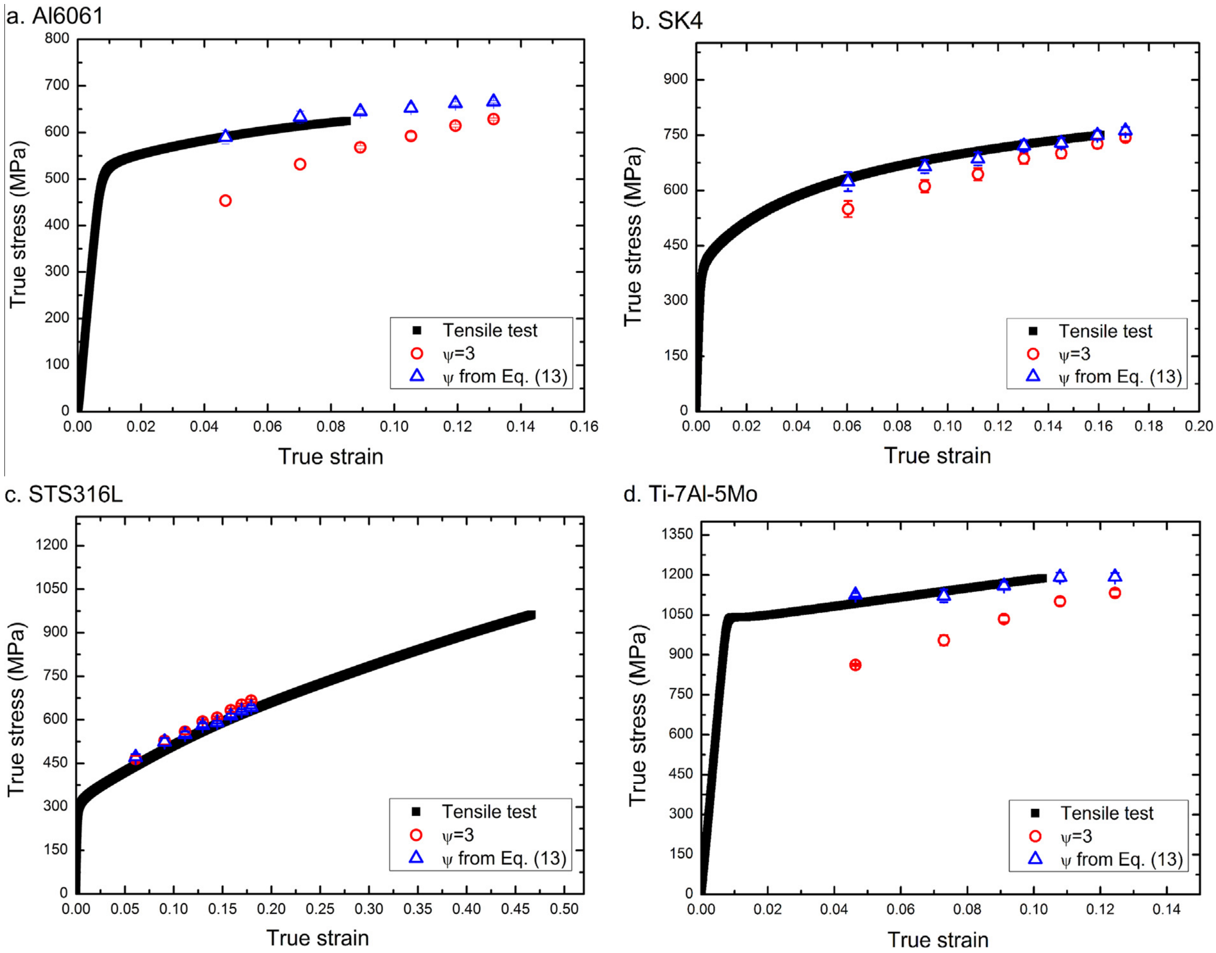

Fig. 4. Uniaxial flow stress–strain curve and representative stress–strain points evaluated by instrumented indentation for (a) Al6061, (b) SK4, (c) STS316L, and (d) Ti–7Al–5Mo.

4.3. Strain-hardening exponent—ratio of loading slope

We analyze Eq. (39) in terms of correlation between flow properties in tension and the indentation load–depth curve. By the definition of mean pressure, we can write

$$L = A \cdot P_m = A \cdot \psi\sigma_t. \tag{41}$$

Here A is given by the contact radius a, the indenter radius R, and the contact depth h as

$$A = \pi a^2 = \pi(2Rh - h^2). \tag{42}$$

Combining Eqs. (7b), (35), (41), and (42) yields the following:

$$L = \pi\psi K \frac{1}{4^n R^n} a^{n+2}. \tag{43}$$

Fig. 5 compares the experimental curve of indentation load L vs. contact radius a and Eq. (43) for Al6061, SK4, STS316L, and Ti–7Al–5Mo; we found good agreement between the indentation load-contact radius curve and points evaluated with mechanical properties in Eq. (43).

To examine the effect of strain-hardening exponent on indentation load in Eq. (43), we derive the indentation load L with respect to contact radius a as

$$\frac{dL}{da} = 2\Pi_1\Pi_2 a + \Pi_1\Pi_3(n+2)a^{n+1}, \tag{44}$$

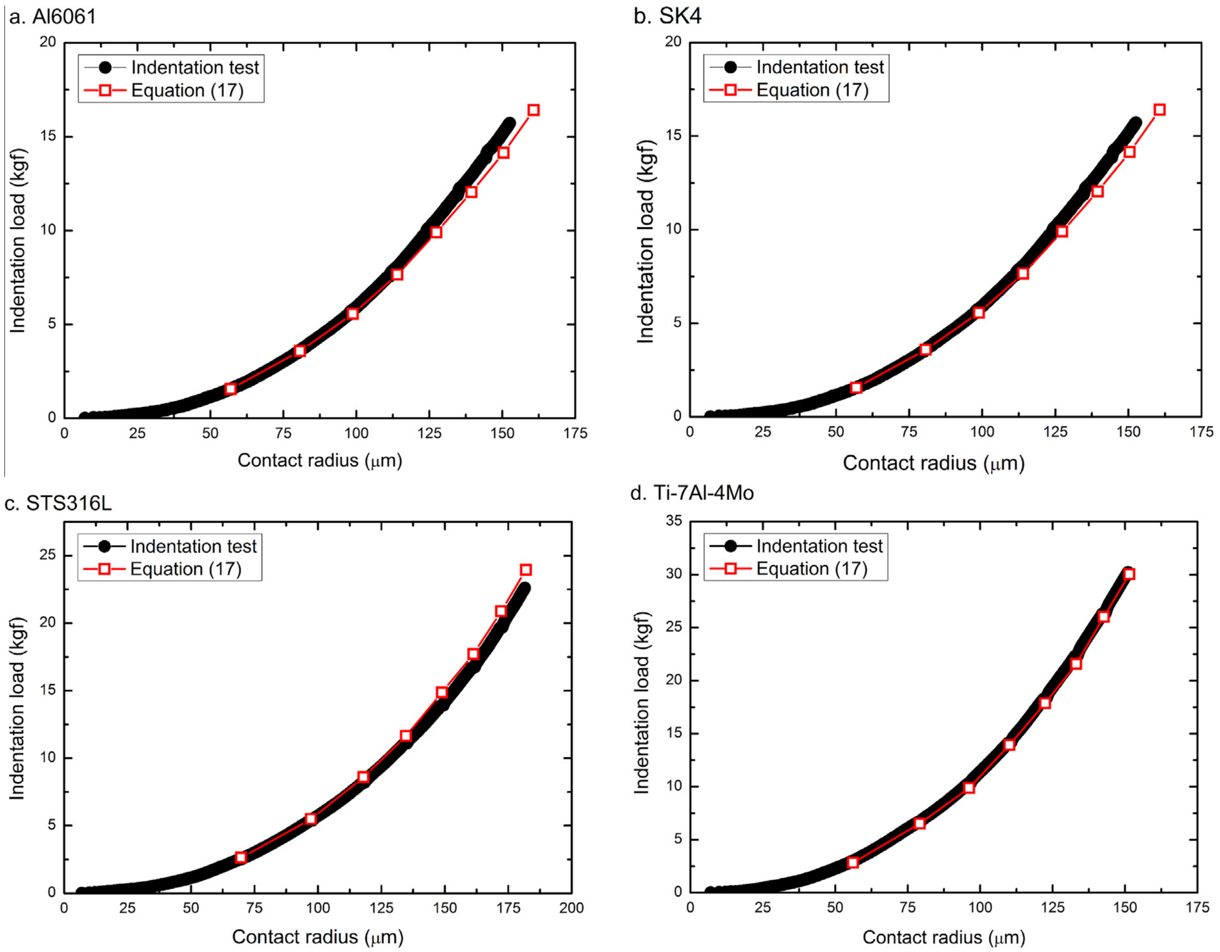

Fig. 5. Contact radius and indentation load in instrumented spherical indentation versis and those evaluated by stress distribution in expanded ECM.

where

$$\Pi_1 = \pi K \frac{1}{4^n R^n}, \tag{44a}$$

$$\Pi_2 = \frac{2}{3}\left(1-\frac{1}{n}\right)\left(\frac{1}{4}\frac{E}{\sigma_y}\frac{1}{R}\right)^{-n}, \tag{44b}$$

$$\Pi_3 = \frac{2}{3}\left(\frac{1}{n}+\frac{3}{2}k\right). \tag{44c}$$

The ratio of slopes p at two arbitrary contact radii a_1 and a_2 is expressed as

$$p = \frac{\left.\frac{dL}{da}\right|_{a_2}}{\left.\frac{dL}{da}\right|_{a_1}} = \frac{2+\frac{\Pi_3}{\Pi_2}(n+2)a_2^n}{2+\frac{\Pi_3}{\Pi_2}(n+2)a_1^n}\cdot\frac{a_2}{a_1}. \tag{45}$$

To understand Eq. (45) simply, the relation between n and p is presented in Fig. 6 for fixed values a_1 = 150 μm, a_2 = 200 μm where R is 250 μm and k is determined from Eq. (40). Fig. 6 shows that the strain-hardening exponent can be evaluated with the parameter p in spite of the small deviation in yield strain from 0.001 to 0.01 for relatively high p. Because the strain-hardening exponent is the amount of increase in hardening slope in uniaxial tension, it is reasonable that it is closely related to the ratio of slopes in indentation loading curve. Fig. 6 compares Eq. (45) and the experimental data for our 13 metals. Most metals show a proportional relation between p and n, as predicted analytically above. The overestimated p which is below the analytic values in Fig. 6 may arise because of an underestimation of k with n in Eq. (40).

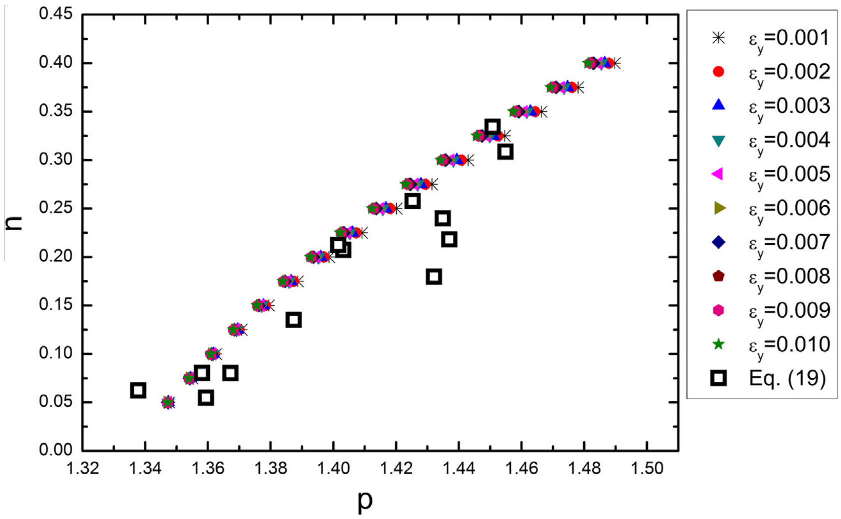

Fig. 6. Strain-hardening exponent as a function of ratio of loading slope from numerical approximation and experimental observation.

4.4. Yield strength—understanding and modifying the Meyer relation

Meyer (1908) found a relation between yield strength and Brinell hardness, now called the Meyer relation, in which indentation load L is given with indenter diameter D and residual diameter d as:

$$\frac{L}{d^2} = C \cdot \left(\frac{d}{D}\right)^{m-2} \tag{46}$$

where C and m are material constants and the Meyer index determined by fitting. George et al. (1976) suggested an empirical linear relationship between yield strength and the material constant:

$$\sigma_y = \beta \cdot C, \tag{47}$$

where the constant β depends on material class; for example, C is reported as 0.224 for the sheet steel grades. The Meyer relation gives a good approximation of yield strength from inspection of the indentation load–depth curve.

To understand the Meyer relation in terms of theoretical analysis, we use the results of stress-field analysis and the constitutive equation as follows. Equation (47) is rewritten with the geometrical relation of the spherical indenter as

$$P_m = \frac{4}{\pi} C \left(\frac{a}{R}\right)^{m-2}. \tag{48}$$

Using Eqs. (1) and (35), Eq. (48) is rewritten as

$$\sigma = \frac{4^{m-1}}{\pi} \frac{C}{\psi} (\varepsilon)^{m-2}. \tag{49}$$

If we consider the constitutive Hollomon equation in Eq. (7b), the strength coefficient and strain-hardening exponent are given by

$$K = \frac{4^{n+1}}{\pi} \frac{C}{\psi_0}, \tag{50}$$

$$n = m - 2. \tag{51}$$

The Hollomon equation implies the following equation at the yield point, where σ_y is the yield strength and E is the yield strain:

$$\sigma_y = K \left(\frac{\sigma_y}{E}\right)^n. \tag{52}$$

Finally, the yield strain can be expressed by combining Eqs. (50) and (52) as

$$\sigma_y = \left(\frac{4^{n+1}}{\pi E^n \psi}\right)^{\frac{1}{1-n}} C^{\frac{1}{1-n}}. \tag{53}$$

This equation implies that the material constant C does not directly determine the yield strain through a characteristic constant, as in Eq. (47). If we regard the multiplying constant of Eq. (53) as β in Eq. (47) and C as $C^{\frac{1}{1-n}}$ in Eq. (47), yield strength is determined not by the simple values of β and C but by the combination of various parameters such as strain-hardening exponent, elastic modulus and plastic constraint factor. The plastic constraint factor is related to yield strain and strain-hardening exponent as discussed above; in particular, it depends strongly on the strain-hardening exponent. The elastic moduli of metallic alloys of similar base metals are almost identical. For this reason, if the materials can be classified on the basis of similar elastic moduli and strain-hardening exponents, the Meyer relation may be applicable. This is why the Meyer relation estimates acceptable yield strengths for similar metal classes. For the 13 metallic materials studied here, we found that Meyer's material parameter β depends on the strain-hardening exponent as shown in Fig. 7a. It thus seems clear that the strain-hardening exponent is the most important parameter in evaluating the yield strength using the Meyer relation.

Even though the conventional Meyer relation yields a good estimate by using a constant dependent on the strain-hardening exponent, Eq. (53) makes it possible to understand the relation between indentation load–depth curve and flow properties. We rewrite Eq. (53) by defining a modified multiplying constant β' as

$$\sigma_y = \beta' C^{\frac{1}{1-n}}. \tag{54}$$

By inputting actual yield strength and indentation data into Eq. (54), we evaluate β' and approximate it as a function of the strain-hardening exponent as in Fig. 7b. As β is well approximated by the strain-hardening exponent, β' is also well described. This analysis suggests that yield strength can be determined through the Meyer relation when materials are classified by strain-hardening exponent.

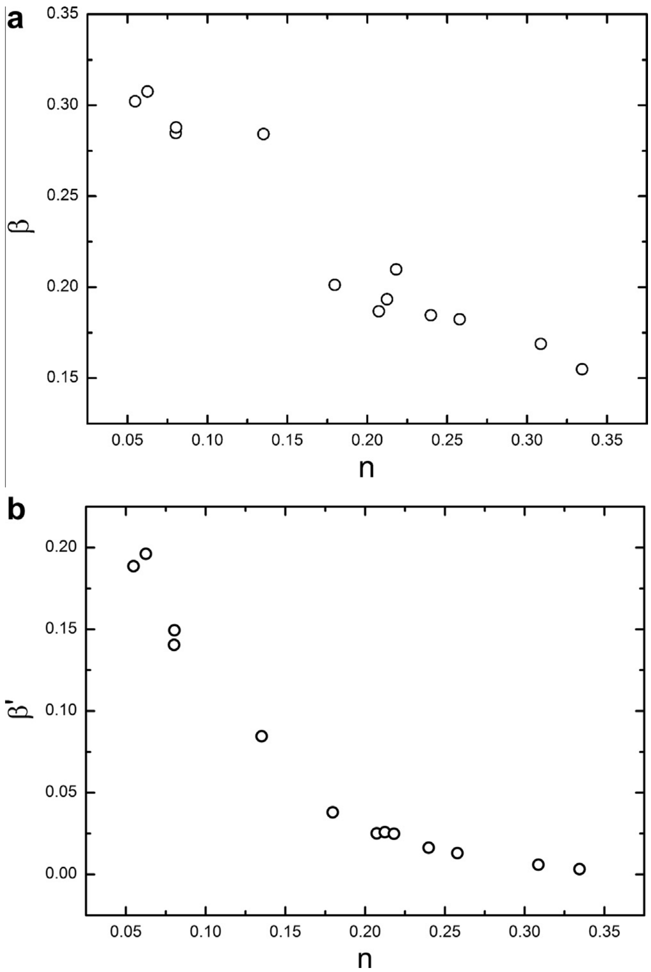

Fig. 7. Dependence of characteristic constant on strain-hardening exponent in (a) Meyer relation and (b) modified Meyer relation.

Table 1
Ratio of slope and estimated strain-hardening exponent.

Materials	p	n	Estimated n	Difference
Al6061	1.3378	0.0625	0.0447	−0.0178
Al7075	1.3581	0.0804	0.0664	−0.0140
API X100	1.3874	0.1351	0.1193	−0.0158
S45C	1.4253	0.2578	0.2140	−0.0439
SK4	1.4321	0.1797	0.2330	0.0533
SKS3	1.4370	0.2181	0.2469	0.0289
SUJ2	1.4349	0.2398	0.2408	0.0010
STS303F	1.4508	0.3344	0.2866	−0.0479
STS316L	1.4549	0.3086	0.2986	−0.0100
STS403	1.4016	0.2124	0.1520	−0.0603
STS420J2	1.4032	0.2073	0.1561	−0.0512
Ti–6Al–4 V	1.3672	0.0802	0.0804	0.0002
Ti–7Al–4Mo	1.3594	0.0548	0.0682	0.0134

Table 2
Estimation of yield strength with modified Meyer relation.

Materials	σ_y (Mpa)	n	$C^{\frac{1}{1-n}}$	σ_y from Eq. (30) (MPa)	Error (%)
Al6061	262	0.0625	1338	242	−7.9
Al7075	518	0.0804	3466	516	−0.4
API X100	667	0.1351	7887	603	−9.5
S45C	363	0.2578	27840	327	−9.9
SK4	406	0.1797	10683	434	6.9
SKS3	435	0.2181	17434	388	−10.9
SUJ2	404	0.2398	24784	388	−4.1
STS303F	341	0.3344	105407	340	−0.2
STS316L	305	0.3086	51237	282	−7.6
STS403	335	0.2124	12954	316	−5.9
STS420J2	398	0.2073	15846	419	5.0
Ti–6Al–4 V	937	0.0802	6670	995	6.1
Ti–7Al–4Mo	1031	0.0548	5463	1070	3.8

4.5. Estimation of strain-hardening exponent and yield strength

It is possible to determine n and σ_y from Eqs (45) and (54) by using the expanded ECM to analyze the stress distribution under the spherical indenter. Each equation contains two independent parameters affecting the determination of uniaxial tensile properties; however, they can be simplified to be functions of the major parameters by numerical approximation, as discussed above. For simple mathematical expressions, we took the third-order polynomial fitting from the experimental results in Figs. 6 and 7 for strain-hardening exponent with ratio of slope and β' of the modified Meyer relation with strain-hardening exponent:

$$n = -52.24p^3 + 228.18p^2 - 329.32p + 157.31, \qquad (55)$$

$$\beta' = -13.43n^3 + 11.53n^2 - 3.42n + 0.36. \qquad (56)$$

Table 1 shows estimates of the strain-hardening exponent from p at indented radii 150 μm and 200 μm with Eq. (55). From analysis of the stress field analysis under the indenter, we give a quantitative relation for the ratio of slope and strain-hardening exponent and suggest a novel way to determine the strain-hardening exponent in instrumented indentation testing. Table 2 shows that the yield strength is well estimated by Eq. (56). This result suggests that yield strength can be determined through the Meyer relation when materials are classified by strain-hardening exponent.

5. Conclusions

To understand the relation between the indentation load–depth curve and tensile properties of materials, we investigated the core condition of the expanding cavity model and found that this model does not fully match the pressure of the core to the indentation mean pressure. By adopting a scaling factor and comparing it at various combinations of strain-hardening exponent, yield strain and indentation strain, we found the following results. First, the additional hardening of the difference between the actual cavity and the model core is almost negligible in explaining the difference between the core pressure and indentation mean pressure. Second, the effect of the strain-hardening exponent dominates that of yield strain because yield strain is related only to the initial yield point and most of the field beneath the indenter has already experienced fully plastic deformation, especially directly beneath the indenter. Third, the hydrostatic pressure condition relies on the self-similar shape of the stress field and is directly correlated to pileup. Thus the strain-hardening effect dominates over the pileup and stress field shape. Materials with relatively low n values generally show greater pileup and similar hemispherical stress-field shapes, and since this corresponds to the expanding cavity model, only minor correction is needed. However, large-n materials like austenitic stainless steels, with linear strain hardening by extra dislocation hardening, show a large mismatch.

By correcting the mismatch at the core using the strain-hardening exponent, we found that the relation between indentation mean pressure and uniaxial flow stress (the so-called *plastic constraint factor*) depends on the materials' flow properties themselves. Predetermination of the strain-hardening exponent and yield strain is required to predict the actual relation from indentation. To alleviate difficulties in the numerical analysis caused by such determinations, we suggested two methods. First, using the result of stress analysis with the corrected expanding cavity model, we successfully described the indentation load–depth curve using flow properties. Second, rom the ratio of the slope of the indentation load and contact radius curve, we derived a quantitative relation of the strain-hardening exponent to the predicted strain-hardening exponent. For evaluation of yield strength, we reviewed the Meyer relation by combining the constitutive equation and indentation stress field analysis and found that the material-dependent constant in the Meyer relation depends on the strain-hardening exponent. Finally, we suggested a modified Meyer relation to predict the yield strength of materials with strain-hardening exponent.

Acknowledgments

This work was supported by the National Research Foundation of Korea (NRF) grant funded by the Korea government (MEST) (2012-0008722).

References

Ahn, J.H., Kwon, D., 2001. Derivation of plastic stress–strain relationship from ball indentations: examination of strain definition and pileup effect. J. Mater. Res. 16, 3170–3178.
Akyuz, F.A., Merwin, J.E., 1968. Solution of nonlinear problems of elastoplasticity by finite element method. AIAA J. 6, 1825–1831.
Alcala, J., Barone, A.C., Anglada, M., 2000. The influence of plastic hardening on surface deformation modes around vickers and spherical indents. Acta Mater. 48, 3451–3464.
Anand, L., Ames, N.M., 2006. On modeling the micro-indentation response of an amorphous polymer. Int. J. Plasticity 22, 1123–1170.
Antunes, J.M., Fernandes, J.V., Menezes, L.F., Chaparro, B.M., 2007. A new approach for reverse analyses in depth-sensing indentation using numerical simulation. Acta Mater. 55, 69–81.
ASTM E8-04, 2002. Standard Test Methods for Tension Testing of Metallic Materials, ASTM Int.
Bigoni, D., Laudiero, F., 1989. The qusai-static finite cavity expansion in a non- standard elasto-plastic medium. Int. J. Mech. Sci. 31, 825–837.
Branch, N.A., Arakere, N.K., Subhash, G., Klecka, M.A., 2011a. Determination of constitutive response of plastically graded materials. Int. J. Plasticity 27, 728–738.
Branch, N.A., Subhash, G., Arakere, N.K., Klecka, M.A., 2011b. A new reverse analysis to determine the constitutive response of plastically graded case hardened bearing steels. Int. J. Solids Struct. 48, 584–591.
Buclille, J.L., Stauss, S., Felder, E., Michler, J., 2003. Determination of plastic properties of metals by instrumented indentation using different sharp indenters. Acta Mater. 51, 1663–1678.
Chadwick, P., 1959. The quasi-static expansion of a spherical cavity in metals and ideal soils. Q. J. Mech. Appl. Math. 12, 52–71.
Chiang, S.S., Marshall, D.B., Evans, A.G., 1982. The response of solids to elastic/plastic indentation. I. Stresses and residual stresses. J. Appl. Phys. 53, 298–311.
Dao, M., Chollacoop, N., Van Vliet, K.J., Venkatesh, T.A., Suresh, S., 2001. Computational modeling of the forward and reverse problems in instrumented sharp indentation. Acta Mater. 49, 3899–3918.
Dumas, G., Baronet, C.N., 1971. Elastoplastic indentation of a halfspace by an infinitely long rigid circular cylinder. Int. J. Mech. Sci. 13, 519–530.
Durban, D., Baruch, M., 1976. On the problem of a spherical cavity in an infinite elasto-plastic medium. J. Appl. Mech. 43, 633–638.
Fornell, J., Concustell, A., Surinach, S., Li, W.H., Cuadrado, N., Gebert, A., Baro, M.D., Sort, J., 2009. Yielding and intrinsic plasticity of Ti–Zr–Ni–Cu–Be bulk metallic glass. Int. J. Plasticity 25, 1540–1559.
Gao, X.L., 2006. An expanding cavity model incorporating strain-hardening and indentation size effects. Int. J. Solids Struct. 43, 6615–6629.
Gao, X.L., Jing, X.N., Subhash, G., 2006. Two new expanding cavity models for indentation deformations of elastic strain-hardening materials. Int. J. Solids Struct. 43, 2193–2208.
George, R.A., Dinda, S., Kasper, S., 1976. Estimating yield strength from hardness data. Met. Prog. 109, 30–33.
Gouldstone, A., Chollacoop, N., Dao, M., Li, J., Minor, A.M., Shen, Y.L., 2007. Indentation across size scales and disciplines: recent developments in experimentation and modeling. Acta Mater. 55, 4015–4039.
Haj-Ali, R., Kim, H.K., Koh, S.W., Saxena, A., Tummala, R., 2008. Nonlinear constitutive models from nanoindentation tests using artificial neural networks. Int. J. Plasticity 24, 371–396.
Hardy, C., Baronet, C.N., Tordion, G.V., 1971. The elasto-plastic indentation of a half-space by a rigid sphere. J. Numer. Methods Eng. 3, 451–462.
Hencky, H., 1924. Zur theorie plastischer deformationen und der hier im material hervorgerufenen nebenspannungen. In: Proceedings of the First International Congress on Applied Mechanics, Delft.
Herbert, E.G., Pharr, G.M., Oliver, W.C., Lucas, B.N., Hay, J.L., 2001. On the measurement of stress–strain curves by spherical indentation. Thin Solid Films 398–399, 331–335.
Hernot, X., Bartier, O., 2012. An expanding cavity model incorporating pile-up and sink-in effects. J. Mater. Res. 27, 132–140.
Hill, R., 1950. The Mathematical Theory of Plasticity. Clarendon Press, Oxford.
Jiang, P., Zhang, T., Feng, Y., Yang, R., Liang, N., 2009. Determination of plastic properties by instrumented spherical indentation: expanding cavity model and similarity solution approach. J. Mater. Res. 24, 1045–1053.
Johnson, K.L., 1970. The correlation of indentation experiments. J. Mech. Phys. Solids 18, 115–126.
Johnson, K.L., 1985. Contact Mechanics, first ed. Cambridge University Press, New York.
Kang, S.K., Kim, J.H., Lee, Y.H., Kim, J.Y., Kwon, D., 2012. Correlation between the plastic strain and the plastic pileup of the instrumented indentation by utilizing the interrupted tensile test. Mater. Sci. Eng. A 535, 197–201.
Kim, J.Y., Lee, K.W., Lee, J.S., Kwon, D., 2006a. Determination of tensile properties by instrumented indentation technique: representative stress and strain approach. Surf. Coat. Tech. 201, 4278–4283.

Kim, S.H., Lee, B.W., Choi, Y., Kwon, D., 2006b. Quantitative determination of contact depth during spherical indentation of metallic materials – A FEM study. Mater. Sci. Eng. A 415, 59–65.
Kim, K.H., Kim, Y.C., Jeon, E.C., Kwon, D., 2011. Evaluation of indentation tensile properties of Ti alloys by considering plastic constraint effect. Mater. Sci. Eng. A 528, 5259–5263.
Kysar, J.W., Saito, Y., 2011. Wedge indentation into elastic–plastic single crystals, 1: Asymptotic fields for nearly-flat wedge. Int. J. Plasticity 27, 1640–1657.
Lawn, B.R., 1998. Indentation of ceramics with spheres: a century after Hertz. J. Am. Ceram. Soc. 81, 1977–1994.
Lee, C.H., Masaki, S., Kobayashi, S., 1972. Analysis of ball indentation. Int. J. Mech. Sci. 14, 417–420.
Lee, H., Lee, J.H., Pharr, G.M., 2005. A numerical approach to spherical indentation techniques for material property evaluation. J. Mech. Phys. Solids 53, 2037–2069.
Lee, K.W., Kim, K.H., Kim, J.Y., Kwon, D., 2008. Derivation of tensile flow characteristics for austenitic materials from instrumented indentation technique. J. Phys. D: Appl. Phys. 41, 074014.
Liu, Y., Varghese, S., Ma, J., Yoshino, M., Lu, H., Komanduri, R., 2008. Orientation effects in nanoindentation of single crystal copper. Int. J. Plasticity 24, 1990–2015.
Lubliner, J., 1990. Plasticity Theory. Macmillan Publishing Company, New York.
Ma, Z.S., Zhou, Y.C., Long, S.G., Lu, C., 2012. On the intrinsic hardness of a metallic film/substrate system: indentation size and substrate effects. Int. J. Plasticity 34, 1–11.
Marsh, D.M., 1964. Plastic flow in glass. Proc. R. Soc. London A279, 420–435.
Mata, M., Casals, O., Alcala, J., 2006. The plastic zone size in indentation experiments: the analogy with the expansion of a spherical cavity. Int. J. Solids Struct. 43, 5994–6013.
Matthews, J.R., 1980. Indentation hardness and hot pressing. Acta Metall. 28, 311–318.
Meyer, E., 1908. Investigations of hardness testing and hardness. Phys. Z. 9, 66–74.
Mulhearn, T.O., 1959. The deformation of metals by vickers-type pyramidal indenters. J. Mech. Phys. Sol. 7, 85–88.
Park, Y.J., Pharr, G.M., 2004. Nanoindentation with spherical indenters: finite element studies of deformation in the elastic–plastic transition regime. Thin Solid Films 447–448, 246–250.
Samuel, K.G., Rodriguez, P., 2005. On power-law type relationships and the Ludwigson explanation for the stress–strain behaviour of AISI 316 stainless steel. J. Mater. Sci. 40, 5727–5731.
Samuels, L.E., Mulhearn, T.O., 1957. An experimental investigation of the deformed zone associated with indentation hardness impressions. J. Mech. Phys. Sol. 5, 125–134.
Shaw, M.C., DeSalvo, D.J., 1970. A new approach to plasticity and its application to blunt two dimensional indenters. J. Eng. Ind. Trans. ASME 92, 469–479.
Shi, Z.F., Huang, B., Tan, H., Huang, Y., Zhang, T.Y., Wu, P.D., Hwang, K.C., Gao, H., 2008. Determination of the microscale stress–strain curve and strain gradient effect from the micro-bend of ultra-thin beams. Int. J. Plasticity 24, 1606–1624.
Skalski, K., 1979. Contact problem analysis of an elastoplastic body, Prace Naukowe Mechanica, z. 67, Warsaw Ploytechnic.
Studman, C.J., Moore, M.A., Jones, S.E., 1977. Correlation of indentation experiments. J. Phys. D: Appl. Phys. 949, 949–956.
Sundararajan, G., Tirupataiah, Y., 2006. The localization of plastic flow under dynamic indentation conditions: I Experimental results. Acta Mater. 24, 565–575.
Tabor, D., 1951. Hardness of Metals, first ed. Clarendon Press, New York.
Tabor, D., 1986. Indentation Hardness and its Measurement, ASTM STP 889. ASTM Press, Philadelphia.
Taljat, B., Zacharia, T., Kosel, F., 1998. New analytical procedure to determine stress–strain curve from spherical indentation data. Int. J. Solids Struct. 35, 4411–4426.
Veprek-Heijman, M.G.J., Veprek, R.G., Argon, A.S., Parks, D.M., Veprek, S., 2009. Non-linear finite element constitutive modeling of indentation into super- and ultrahard materials: the plastic deformation of the diamond tip and the ratio of hardness to tensile yield strength of super- and ultrahard nanocomposites. Surf. Coat. Tech. 203, 3385–3391.
Yang, D.Y., Lim, T.W., Son, Y., Barlat, F., Yoon, J.W., 2011. Gripless nanotension test for determination of nano-scale properties. Int. J. Plasticity 27, 1527–1536.
Yoffe, E.H., 1982. Elastic stress fields caused by indenting brittle materials. Philos. Mag. A 46, 617–628.